Journal of the Brazilian Society of Mechanical Sciences and Engineering (2024) 46:702
https://doi.org/10.1007/s40430-024-05269-z

TECHNICAL PAPER

Thermal studies on cryocooler thermal masses from 4 K to 300 K for MRI applications

Sushanth R. Shetty[1] · Ruturaj A. Umaranikar[2] · S. Kasthurirengan[3] · Shiva Kumar[1]

Received: 6 April 2024 / Accepted: 26 October 2024
© The Author(s) 2024

Abstract

Gifford–McMahon (GM) cryocoolers are pivotal for maintaining the temperature of MRI magnets, necessitating regular servicing for optimal performance and longevity. This study explores the geometric dimensions and shapes of superconducting magnets utilized in MRI for system cooling. The investigation demonstrates that warm-up time is contingent on heat capacity rather than geometric shapes. As a result, the design of magnets can be customized to specific shapes and sizes in accordance with favorable conditions, given that warm-up time is solely dependent on heat capacity. The primary focus is to deliberately prolong the warm-up time of the magnet relative to the GM cryocooler, consequently minimizing service intervals. Laboratory evaluations explore the use of thermal masses equivalent to MRI magnets, employing typical materials such as copper and aluminum. These masses are cooled to 4 K and then subjected to different heating powers to evaluate warm-up characteristics. Various configurations and shapes of thermal masses are numerically studied for warm-up analysis. Comparative assessments between experimental results and simulations reveal that, for cylindrical thermal masses, 80 W heating power facilitates a 76% reduction in warm-up time compared to 20 W heating across all cases. In the exploration of different geometric thermal masses, aluminum demonstrates a remarkable 35% decrease in warm-up time compared to copper. A noteworthy finding emerges, indicating that warm-up time is contingent on heat capacity rather than geometric shapes. These insights hold substantial relevance, particularly in systems with large thermal capacities, such as superconducting magnets. The study contributes valuable knowledge to the optimization of GM cryocoolers for enhanced MRI magnet performance and extended operational life.

Keywords GM (Gifford–McMahon) cryocooler · MRI magnet · Thermal mass · Warm-up time · Conical

Abbreviations

BSCCO	Bismuth strontium calcium copper oxide
Er_3Ni	Erbium nickel
GE	General electric
GM	Gifford–McMahon
HTS	High-temperature superconductivity
Hz	Hertz
JT	Joule Thomson
K	Kelvin
kW	Kilo Watt
MRI	Magnetic resonance imaging
MW	Mega Watt
NbTi	Negative bias temperature instability
NMR	Nuclear magnetic resonance
PT	Pulse tube
PV	Pressure volume
REBCO	Rare-earth barium copper oxide
W	Watt

Technical Editor: Guilherme Ribeiro.

✉ Shiva Kumar
shiva.kumar@manipal.edu

[1] Department of Mechanical and Industrial Engineering, Manipal Institute of Technology, Manipal Academy of Higher Education, Manipal 576104, India

[2] Voxelgrids Innovations Pvt Ltd, Bangalore, India

[3] Centre for Cryogenic Technology, Indian Institute of Science, Bangalore, India

1 Introduction

Cryocoolers serve as the apparatus responsible for producing essential refrigeration at precise cryogenic temperatures. The term tabletop is used, typically for smaller systems that have an input power of less than 20 kW. It is observed that few systems have input power as low as 2–3 W [1]. Large

Published online: 15 November 2024

systems known as cryogenic refrigerators with input power as high as 1 MW are typically utilized for chilling the superconducting magnets present in the particle accelerators. The working substance used is helium which undergoes a thermodynamic cycle. Six types of cryocoolers that are frequently used are separated into two categories: (1) recuperative cycles and (2) regenerative cycles. The three most common recuperative cycles include Joule Thomson (JT), Claude, and Brayton cycle, and the three most regenerative cycles are Stirling, pulse tube (PT), and Gifford–McMahon (GM). They are offered on the market and utilized for a variety of purposes. GM-type pulse tube cryocoolers and GM cryocoolers, among the different cryocooler systems, operate at low operational frequencies and can produce exceptionally low temperatures.

In the above GM cryocooler shown in Fig. 1, a form of regenerative cycle, chilling at the cold end is accomplished using pressure oscillatory flow with the proper phase angles in between both the pressure and mass flow. Usually, the GM cryocooler runs at 1–2 Hz. The cryocoolers use helium as the working medium to obtain the cold zone's lowest temperature [1]. In the second-stage displacer, the lowest temperature on the order of 4 K is attained when lead is used as the regenerator material [2]. However, this temperature is lowered to 4 K when rare-earth-based regenerator materials are used. The mesh in the first stage displacer of a GM cryocooler plays a critical role in optimizing the cooling efficiency and performance of the cryocooler by facilitating heat exchange and maintaining proper gas flow characteristics. The first stage displacer usually contains meshes of different materials such as copper and brass. Usually, the mesh sizes in the range from 100 to 200 are chosen. At the end and top of the first stage usually, coarser meshes are kept whereas finer meshes are placed at its center.

Since 1990, major developments in low-temperature cryogenics have been engaged using regenerator-based materials such as lanthanides. Erbium nickel (Er_3Ni) which has a higher heat capacity in the 4 K range [2, 3]. This was the first material to be used in two-stage cryocoolers. Toshiba scientists reduced the range of the GM cryocooler from 10 K to 4.2 K by these modifications in the regenerator material. Later other lanthanide materials such as $HoCu_2$ were also used for cooling down to 4 K [4]. In the present study, standard Sumitomo GM cryocooler model SRDK-415D with F50H compressor has been chosen, and the system can be used to cooldown to 4.2 K and warm up to room temperature. Different geometrical shapes of thermal masses prepared from copper and aluminum have been used on the second-stage cold head of the mentioned cryocooler.

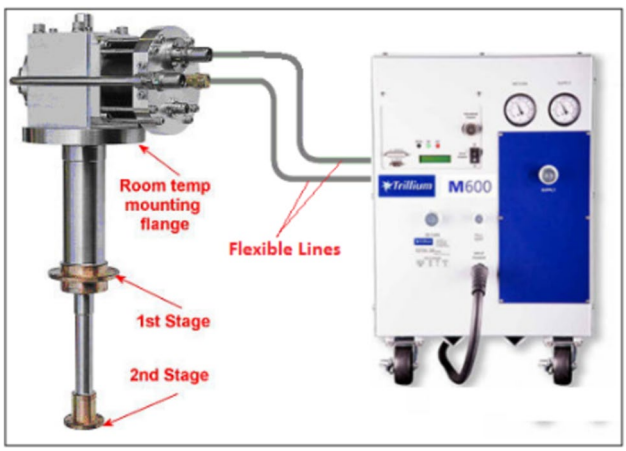

Fig. 1 GM cryocooler

2 Literature review

Cryocooler advancements were closely aligned with the development of GE's MRI systems, especially during the 1980s and 90 s, when cryocoolers were integrated into MRI setups due to enhanced reliability and performance [5]. Despite the potential for open magnet designs to drive this collaborative progress, the MRI system's success is jeopardized by challenges related to initial cost and performance inconsistency, underscoring the significance of manufacturers excelling in these aspects to expand MRI application [5]. This paper explores the essential criteria for choosing cryogenic cooling systems for superconducting machines, emphasizing design, operational, and condition monitoring considerations. It provides guidance for electric machine engineers and designers on the crucial cryogenic factors involved in cooling system selection [6]. Topics covered include typical cooling system configurations, different cryogenic fluids, heat load parameters, and safety margins. Additionally, the paper discusses the importance of auxiliary devices such as heat exchangers and pumps and examines specific challenges in aerospace, naval, and wind energy applications, highlighting unique priorities like weight, cost, and mass efficiency [6].

Superconducting magnet technology has been revolutionized by the utilization of HTS such as BSCCO and REBCO by Bagdinov et al. [7], which has resulted in higher magnetic fields and increased operating temperatures. The progress made in addressing these challenges for BSCCO and REBCO conductors is emphasized, with applications in high-field environments, NMR, MRI, and maglev trains. Despite improvements, concerns related to thermal runaway continue to exist for REBCO magnets, with advancements in Bi2212 and Bi2223 offering potential solutions for high-field, high-density HTS magnets [7].

Grover et al. [8] emphasized that MRI has a significant impact on medical diagnosis, offering a radiation-free alternative and being widely used in clinical practice. They also

proposed MRI principles and clinical applications including parallel imaging and diffusion-weighted imaging [8]. Choi et al. [9] investigated a 1.5 T cryogen-free superconducting magnet featured in a dedicated orthopedic MRI system, cooled by a compact cryostat equipped with a pulse tube cold head offering 1 W cooling power at 4.2 K. Despite requiring a 100-h cooldown time, the magnet achieves stable operation, maintaining magnetic field stability below 0.01 ppm/h.

An in-depth theoretical examination of the Gifford–McMahon cycle is delineated herein [10]. Formulas elucidating the ideal refrigeration output and the figure of merit are meticulously crafted. Moreover, the analysis incorporates an exploration of diverse losses inherent in practical machinery, with corresponding equations meticulously derived to accommodate these losses.

The development of cryocooler technology has made it widely used in laboratories, businesses, and space projects of many kinds. These kinds have increased their applications over the past 20 years as a result of particular requirements and modern trends that emphasize efficiency, regenerative cooling, and problem solving. Meanwhile, ongoing research focuses on cryogen-free 4 K systems and micro-cryocoolers [11]. A thorough investigation is conducted, covering the Gifford–McMahon cycle-based principles, designs, and applications of cryocoolers by Radovinsky et al. [12]. For cryogenics researchers and engineers, key ideas, operational details, and practical considerations were presented, providing helpful insights to improve understanding of cryocooler capabilities and limitations.

In order to maintain IBA S2C2 cyclotron magnet cryocoolers on-site, a method that involves applying targeted heat to certain stages and validating it through numerical optimization and trials was devised by Webber et al. [13]. To minimize service disruption in conduction-cooled superconducting magnets, an alternative method was proposed, involving electric heaters attached to cold head stations. This method permits warming the cold head and body while maintaining cryogenically cooling the cold mass, improving cooling system effectiveness, streamlining maintenance, and decreasing downtime.

Gifford–McMahon cryocoolers are addressed by Sumitomo Heavy Industries which leads to the significant reduction of oscillations and the extension of cooldown time [14]. Thermal links and relief valves were used to optimize the cooldown process, which led to a significant reduction in the cooldown time below 10 K while maintaining the damping effect. This has advantages for cryocoolers that support superconducting devices [14]. Through structural and operational improvements, the performance of a high-capacity GM cryocooler has been improved by Ackermann et al. [15]. This led to better cooling capacities, decreased maintenance requirements, and suitability for a variety of applications, including hydrogen liquefaction and chilling HTS devices. Wang et al. [16] investigated Cryomech Model AL630, a single-stage GM cryocooler, optimized for chilling temperatures between 20 and 30 K, making it appropriate for hydrogen liquefaction and cooling HTS devices. A two-stage GM cryocooler was developed and tested by Wang et al. [17]. It was equipped with precisely timed rotary valves to maximize PV work, allowing it to achieve low temperatures (8.8 K ~ 9 K) within specified time frames. Its heat transfer assessment, thermal load predictions, and compliance with international standards proved its applicability in energy-efficient large display and semiconductor manufacturing processes.

This paper details the design and construction of a 1.5 T head-only MRI superconducting magnet at Wuhan National High Magnetic Field Center, utilizing liquid helium bath-cooling with NbTi wire. The magnet, consisting of nine discretized coils on stainless steel formers, operates at 510 A with a peak field below 3.0 T, a load line under 50%, and a temperature margin above 1 K. A precise thermal load evaluation, crucial for zero boil-off operation, is conducted using finite element analysis, theoretical, and empirical calculations. The heat load results, 0.237 W for the second stage and 20.26 W for the first stage, are within the SRDE-412D4 cryocooler's cooling capacity [18].

This study details the design, construction, and testing of a 1.5 T cryogen-free niobium–titanium whole-body magnet with an 850 mm bore for clinical MRI use. The magnet, which is actively shielded and passively shimmed, confines the 0.5 mT stray field to 2.5/4 m radial/axial positions and achieves 12.1 ppm field inhomogeneity over a 45 mm spherical volume. It uses a two-stage Gifford–McMahon cryocooler to maintain a temperature below 5.7 K. The MRI scanner, equipped with this magnet, demonstrated stable performance and produced high-quality, high-contrast images [19].

This paper outlines the design and optimization of a GM cryocooler for horizontal operation at liquid helium temperatures, based on the KDE420 model. Enhancements included optimizing the second-stage regenerator and displacer stroke length for vertical cooling capacity and using a spring support structure for horizontal performance. The optimized cryocooler achieved 2.60 W vertically and 2.30 W horizontally at 4.20 K, with reduced performance degradation from 0.85 W to 0.28 W. A 570-h test confirmed stable performance, with cooling capacities of 45.0 W at 38.0 K and 2.20 W at 4.20 K, and a FOM of 3.28% in horizontal operation. This approach guides the design of high-capacity GM cryocoolers for horizontal use at low temperatures [20].

This paper details the thermal analysis and cooldown time estimation for a 1.5 T liquid helium-free whole-body MRI superconducting magnet, which uses solid thermal links with a two-stage GM cryocooler. The findings show that

the thermal shield cools to 45.44 K in about 309 h, while the superconducting magnet, precooled to 77 K with liquid nitrogen, reaches 3.73 K after around 372 h. This approach effectively achieves superconducting temperatures without the need for liquid helium [21].

Despite the authors' exploration of abundant configurations as a means of reaching the lowest temperature, there is still a lack of comprehensive knowledge on the warm-up of thermal masses equivalent to MRI. Furthermore, it is crucial to emphasize the dependency of warm-up time with the alterations in the shape and size of thermal components. In addition, studies related to the importance of thermal capacity in controlling warm-up times for various configurations and shapes of thermal masses are also scanty in the available literature.

This has inspired us to construct and test the influence of various arbitrary shapes and sizes that affect the warm-up of the thermal masses equivalent to MRI. Hence in the present work, various thermal masses of different configurations (shapes) are utilized, incorporating common materials such as copper and aluminum. These thermal masses are initially cooled to the lowest temperature (4 K) and subsequently allowed to warm up. The warm-up process of the different thermal masses was also analyzed using commercially available ANSYS software and compared with the experimental results.

3 Experimentation

3.1 Experimental and theoretical analysis of cylindrical thermal masses

In this study, a standard Sumitomo GM cryocooler model SRDK-415D is utilized. The system's warm-up time was found to be lengthy, particularly when transitioning from a cooled state to room temperature. To expedite the warming process, cartridge heaters are introduced, varying in wattage (20 W, 40 W, 60 W, and 80 W), serving as heaters to hasten the heating of thermal masses.

Four cylindrical thermal masses were fabricated shown in Fig. 2a and b, two composed of copper and two of aluminum, respectively. These were designed to enable the analysis of warm-up behavior for individual thermal masses as well as for thermal masses stacked on top of each other.

3.2 A. Temperature measurement

For cold head temperature measurements, silicon diodes (Si410C) and diode sensors were employed to monitor temperature changes. Diode sensors were created by integrating emitter and collector components from typical transistors such as BC107A and BC109. Calibration of these diodes was conducted using Si410C. After the production of thermal masses, as shown in Fig. 3a and b, they were mounted to carry out experiments, with temperature sensors also affixed.

3.3 B. Experimental procedure

The experimental procedure involved several key steps:

- Initially, when the system was powered on, the vacuum pump was activated to evacuate the vacuum jacket, with pressure readings displayed on a gauge.
- Once the vacuum jacket reached an appropriate vacuum level, the helium compressor was started, allowing the displacer to move and initiating cold head refrigeration.
- Subsequently, as the vacuum level decreased to sufficiently low values, cryopumping commenced, leading to the closure of the pumping valve in the vacuum system. Temperature monitoring continued until it reached 4 K.
- To expedite the warm-up process, cartridge heaters were applied with wattages of 20 W, 40 W, 60 W, and 80 W, as per the requirement.

(a) (b)

Fig. 2 **a** and **b** provide visuals of the thermal masses, base plate, and radiation shield made from aluminum and copper

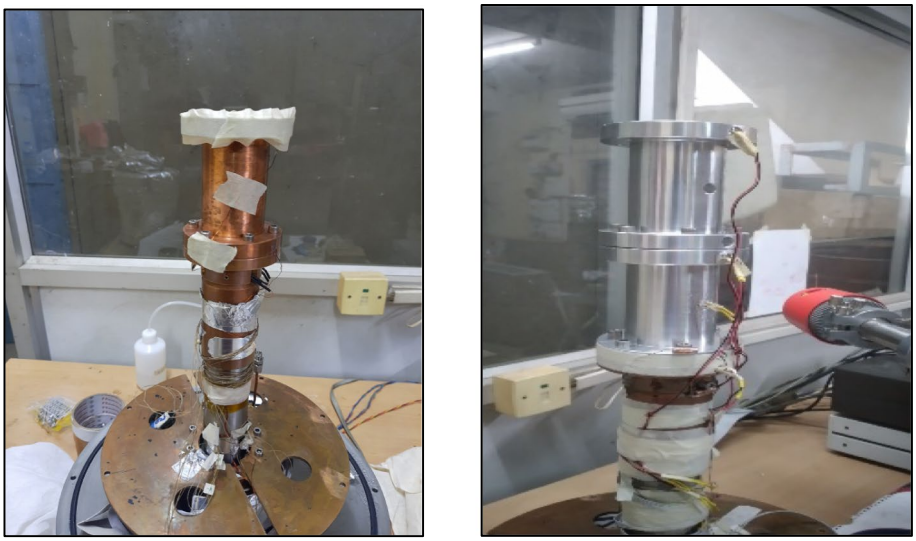

(a) **(b)**

Fig. 3 **a** and **b** Single and stacked thermal masses assembled on the cold head with temperature sensors

Fig. 4 Experimental setup **(1)** Cryocooler **(2)** Turbomolecular pump **(3)** Compressor **(4)** Temperature controller **(5)** Constant current source **(6)** Pressure gauge **(7)** DAQ (Data Acquisition system) **(8)** PC {LabVIEW program} **(9)** Chiller unit

- Data acquisition through a computer system monitored the temperatures of thermal mass warm-up over time, maintaining constant current and voltage.

The LabVIEW program on the computer was employed to collect and subsequently present the data graphically. Figure 4 shows the experimental setup to warm up the thermal masses.

3.4 C. Data analysis and comparison

All diodes exhibited reliable readings, facilitating further studies. Calibration of diodes enabled the generation of temperature versus voltage graphs to determine the appropriate slope. These data were used to derive polynomial equations for temperature calculations in both stages, subsequently resulting in graph-based outcomes. These experimental results were then compared with theoretical analysis.

The experiments were structured in the following sequence: single aluminum thermal mass, single copper thermal mass, stacked aluminum thermal mass, stacked copper thermal mass, stacked aluminum–copper (Al-Cu) thermal mass, and stacked copper–aluminum (Cu-Al) thermal mass. The theoretical analysis was carried out using ANSYS software, and the comparison of theoretical and experimental analysis of cylindrical thermal masses was conducted. Notably, the analysis was comparable when considering a specific factor, which is elaborated upon in the Results and Discussion section.

3.5 Theoretical analysis of different geometrical shapes

3.6 A. Design of arbitrary thermal mass geometries:

Considering the factor term's influence on the comparability of theoretical and analytical results for cylindrical thermal masses, the concept emerged that experimenting with different shapes of thermal masses theoretically could potentially streamline manufacturing processes.

Building upon the design of cylindrical thermal masses, dimensions for various arbitrary shapes of thermal masses were created using SolidWorks and CATIA software. The aim was to investigate whether the warm-up of thermal masses was shape dependent. Basic geometries, including conical, spherical, and cuboid shapes, were prepared as shown in Fig. 5. Within the scope of conical structures, one end was fixed at 50 mm, while the other end was varied to dimensions of 10 mm, 20 mm, 30 mm, and 40 mm, allowing for exploration of different conical geometries.

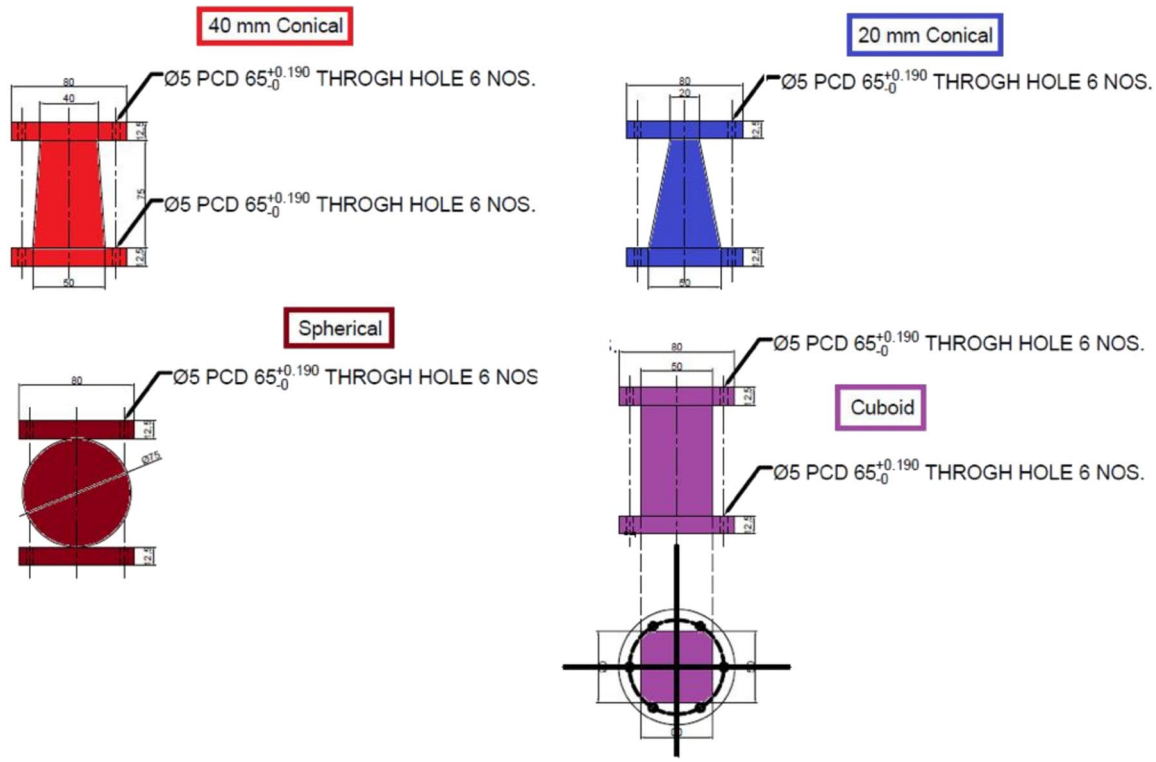

Fig. 5 2D diagrams of conical, spherical, and cuboidal thermal masses

3.7 B. Transient thermal analysis using ANSYS workbench

To obtain theoretical results and enable comparison with experimental data, a transient thermal analysis was conducted using ANSYS Workbench. The process began by selecting the appropriate engineering data, wherein two materials, copper and aluminum, were chosen. These materials were characterized by their respective physical and thermal properties, including density, thermal conductivity, and specific heat. The densities for copper and aluminum were specified as 8960 kg/m^3 and 2710 kg/m^3, respectively. The thermal conductivity for aluminum was set at 237 W/mK, whereas the thermal conductivity for copper varied with temperature, as illustrated in Fig. 6.

Similarly, the specific heat of both copper and aluminum changes with temperature, as shown in Fig. 7a and b, respectively.

Following the assignment of engineering data, the necessary external geometry was imported, which had been preprepared using CATIA software. During the import process, it was essential to specify "Add Material" instead of

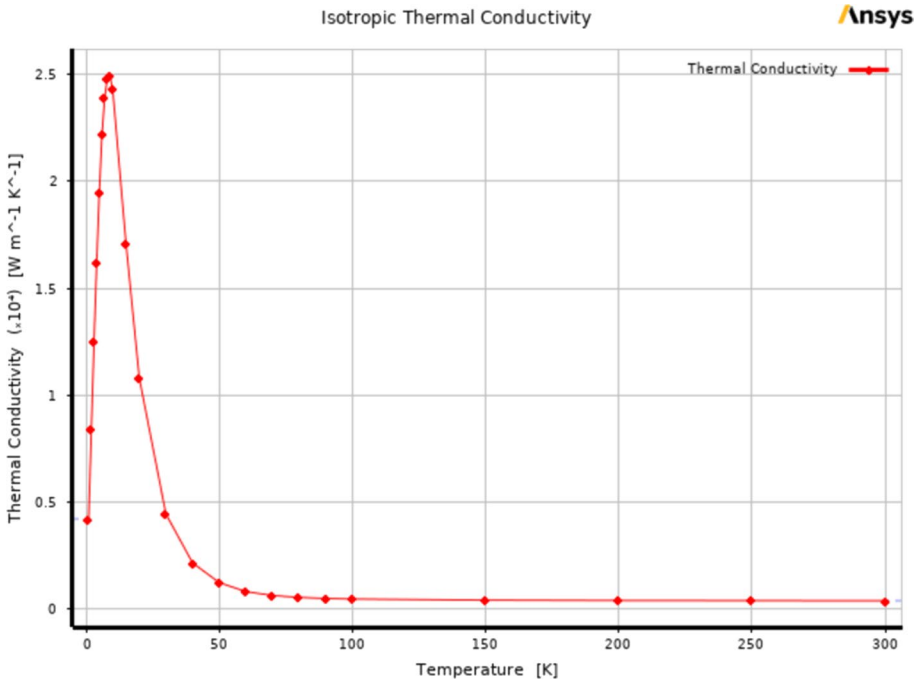

Fig. 6 Thermal conductivity for copper

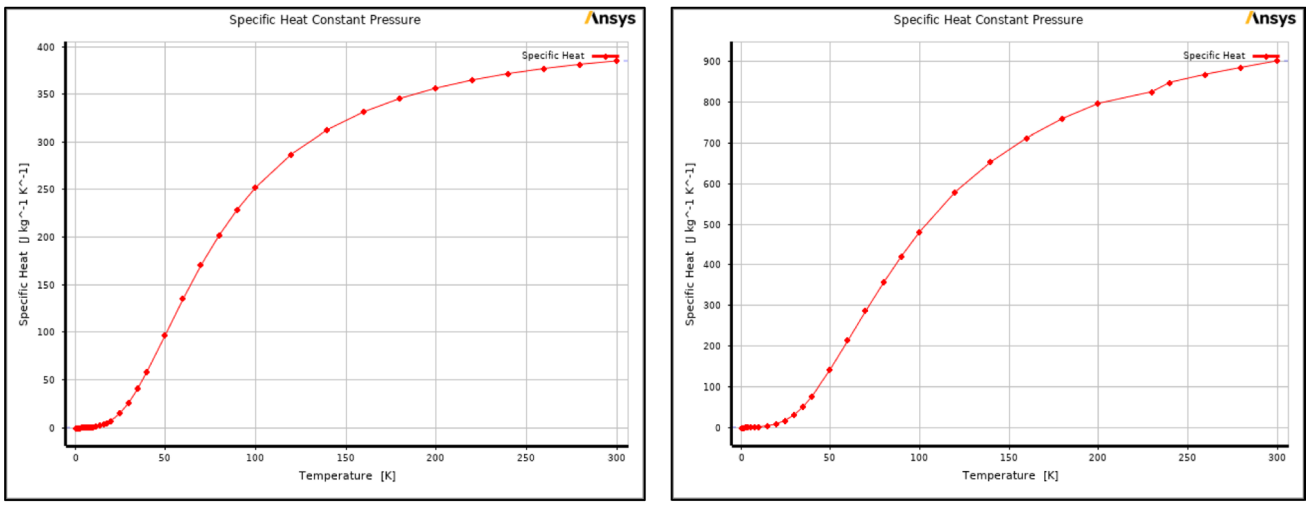

(a) (b)

Fig. 7 Specific heat of **a** copper and **b** aluminum

"Add Frozen" in the operation section before generating the model. One side of the thermal mass, where the heater was to be applied, was selected and labeled as "Heater."

Following geometry selection, material properties (copper or aluminum) were assigned based on the engineering data. To ensure grid independence [22], a grid refinement study was conducted on a stacked copper thermal mass subjected to a 60 W heat load. Various element sizes were evaluated, including 2 mm, 5 mm, 10 mm, 25 mm, and 50 mm. As depicted in Fig. 8, element sizes larger than 2 mm exhibited significant variations in results, while those smaller than 2 mm yielded consistent outcomes but required excessive computational time. Consequently, an element size of 2 mm was determined to be the optimal choice for this analysis.

For the transient thermal analysis, heat flow was added, with an initial temperature set to 5 K. The number of analysis steps varied depending on the material and thermal mass. For aluminum, three steps were sufficient due to its shorter warm-up time, whereas for copper and stacked thermal masses, five steps were required. The maximum end time was set to 6000 s for aluminum, and 10,000 s for stacked copper, based on preliminary analyses. The auto time-stepping feature was program controlled.

After setting all analysis parameters, heat flow was added by selecting the geometry and the named selection, followed by assigning the heater with power levels of 20 W, 40 W, 60 W, and 80 W, as required. In the final solution section, temperature results were inserted, as the output was presented in terms of temperature variation. It is important to note that no radiation effects were considered in the analysis of the thermal mass. The analysis was then executed, yielding time-dependent data on the minimum and maximum temperatures. This data were subsequently used to plot graphs for various shapes and sizes of thermal masses, leading to the generation of the warm-up plot. Meshed models for ANSYS analysis of various geometrical shapes are depicted in Fig. 9.

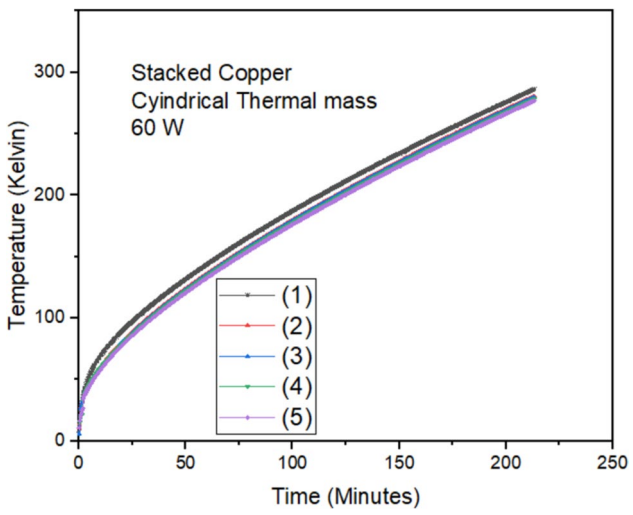

Fig. 8 Grid independence test (1): 50 mm mesh element size, (2): 25 mm mesh element size, (3): 10 mm mesh element size, (4): 5 mm mesh element size, (5): 2 mm mesh element size

Upon analyzing the collected data, a comparison of warm-up times for thermal masses of different geometrical shapes with respect to their mass revealed an intriguing observation. Warm-up times were found to be directly dependent on the mass of the specific material, such as copper or aluminum, rather than the geometrical shape of the object. This suggests that warm-up times are primarily influenced by the thermal capacity of the material, particularly when comparing different materials like copper and aluminum.

4 Results and discussion

4.1 Experimental and theoretical analysis of cylindrical thermal masses

This study presents a comprehensive investigation involving both experimental and theoretical analyses of diverse configurations of cylindrical thermal masses. The focus of this research lies in the exploration of copper and aluminum materials, integral to understanding the thermal dynamics of the studied masses. Standard analytical procedures were employed to obtain the results presented in this study. The governing equations utilized are detailed in Ref. [23]. For a comprehensive understanding of the methodology, readers are encouraged to consult this reference.

4.1.1 Experimental analysis of cylindrical thermal mass

Experimental analysis was conducted on various configurations, including single aluminum, single copper, stacked aluminum, stacked copper, and stacked aluminum–copper (Al-Cu) and copper–aluminum (Cu-Al) composites. All thermal masses were initially cooled to approximately 4 K and subsequently heated using different power levels: 20 W, 40 W, 60 W, and 80 W, until reaching room temperature. To minimize experimental duration, the maximum time was capped at 200 min for the 20 W heating power. Figure 10a and b illustrates the experimental warm-up profiles for various heat loads in the case of single cylindrical aluminum and copper specimens.

The results indicate that higher wattage leads to shorter warm-up times, with aluminum exhibiting a faster warm-up rate compared to copper. Different colors in the graphs represent distinct sensors and diodes mounted on the thermal masses. In the case of stacked sensors, a total of 5 sensors were utilized, while for the single thermal mass,

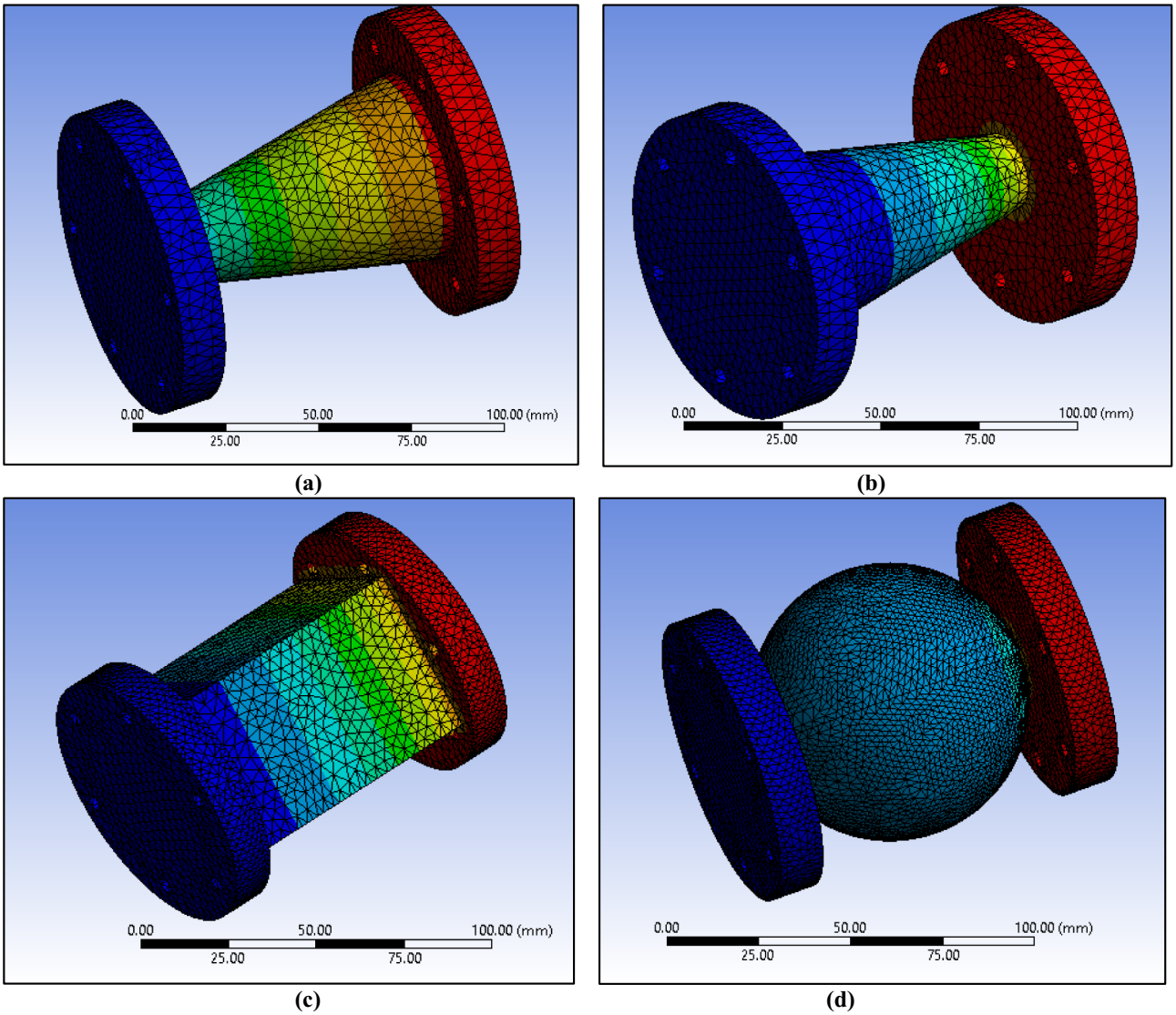

Fig. 9 Meshed models for ANSYS analysis **a** conical, **b** reverse conical, **c** cuboidal, and **d** spherical

only 3 sensors were employed. Figure 11a–d illustrates the experimental warm-up characteristics under different heat loads for stacked aluminum, stacked copper, and stacked aluminum–copper (Al-Cu) and copper–aluminum (Cu-Al) composites.

Comparing single and stacked thermal masses reveals that stacked configurations require longer warm-up times. Among stacked thermal masses, stacked aluminum exhibits the shortest warm-up duration, while stacked copper requires the most time to reach the desired temperature. Stacked aluminum–copper (Al-Cu) and copper–aluminum (Cu-Al) composites display nearly identical warm-up profiles at higher heat power levels (60 W and 80 W). Table 1 presents the experimental time required for single and stacked thermal masses of copper and aluminum to reach 200 K. In all cases, 80 W heating power takes approximately 76% less time to warm up compared to 20 W heating.

4.1.2 Theoretical analysis of cylindrical thermal masses

Theoretical analysis was conducted using ANSYS software, paralleling the experimental conditions with heating power levels of 20 W, 40 W, 60 W, and 80 W. Figure 12a–d illustrates the theoretical warm-up data for single and stacked thermal masses of copper and aluminum for cylindrical thermal masses.

Similar to the experimental data, theoretical results indicate that copper requires more time than aluminum, and stacked thermal masses require more time than single thermal masses. Table 2 shows the theoretical time required for single and stacked thermal masses of copper and aluminum

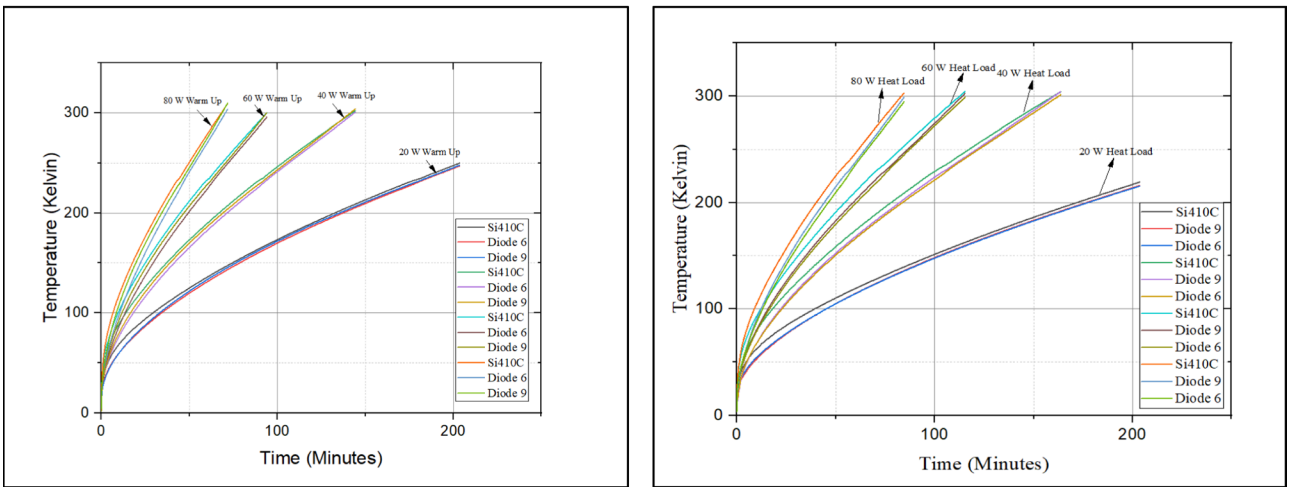

(a) **(b)**

Fig. 10 Experimental warm-up plots of the single cylindrical shaped thermal mass **a** aluminum and **b** copper

to reach 200 K. In all cases, 80 W heating power takes approximately 76% less time to warm up compared to 20 W heating.

4.1.3 Comparison of experimental and theoretical analysis of cylindrical thermal masses

The comparison between experimental and theoretical analyses unveils an interesting aspect of the warm-up characteristics. Notably, the experimental warm-up times were consistently observed to be longer than their theoretical counterparts.

The ANSYS analysis which considers the variation in specific heat with temperature of the thermal masses is essential to understand the experimental results. Further, since the thermal masses are relatively short in length and the ΔT within thermal mass is only few kelvins. Hence, the effect of thermal conductivity variation of the thermal mass with temperature can be neglected in the analysis. The factor $\varepsilon F \varepsilon$ represents the ratio of the experimental time to the time predicted by the theory to reach a given temperature.

So equation can be written

$$F = t_{\exp}/t_{th} \tag{1}$$

The experimental system was compared with that of the theoretical analysis in Fig. 13. The first part (a) of the drawing shows the model chosen for the theoretical analysis while the second part (b) represents the actual experimental system.

If A be the thermal capacity of the thermal masses attached to the cold head and C is thermal capacity of the components till the first stage below the second-stage cold head. Hence it can be written as

$$F = \frac{(A + C)}{A} \tag{2}$$

$$\text{i.e. } F.A = A + C \tag{3}$$

$$\text{or } C = A(F - 1) \tag{4}$$

The factor F for different experimental conditions is presented in Table 1, showcasing that experimental analysis takes F times more time to warm up than theoretical analysis. Noteworthy cases, values marked with an asterisk (*) indicate data points that were deemed unreliable due to inconsistencies or measurement errors. Specific ranges of thermal capacities for different configurations are summarized in Table 3.

Table 4 presents the percentage deviation between the experimental and theoretical results, expressed as a positive or negative value. It is observed that the deviation is consistently below ± 5% and two data points were excluded.

Equation (4) allows estimation of C from the value of F, as depicted in Table 5. The value of A can be estimated by considering the dimensions of the thermal masses, along with their density and specific heat values.

Three specific cases (copper 80 W, stacked copper 40 W, and stacked Al-Cu 20 W) exhibit deviations from the established trend. These outliers are marked with an asterisk (*) and are considered errors. The remaining C values in Table 5, representing both aluminum and copper materials, fall within the range of 980 to 1250. It is essential to acknowledge the presence of an additional thermal

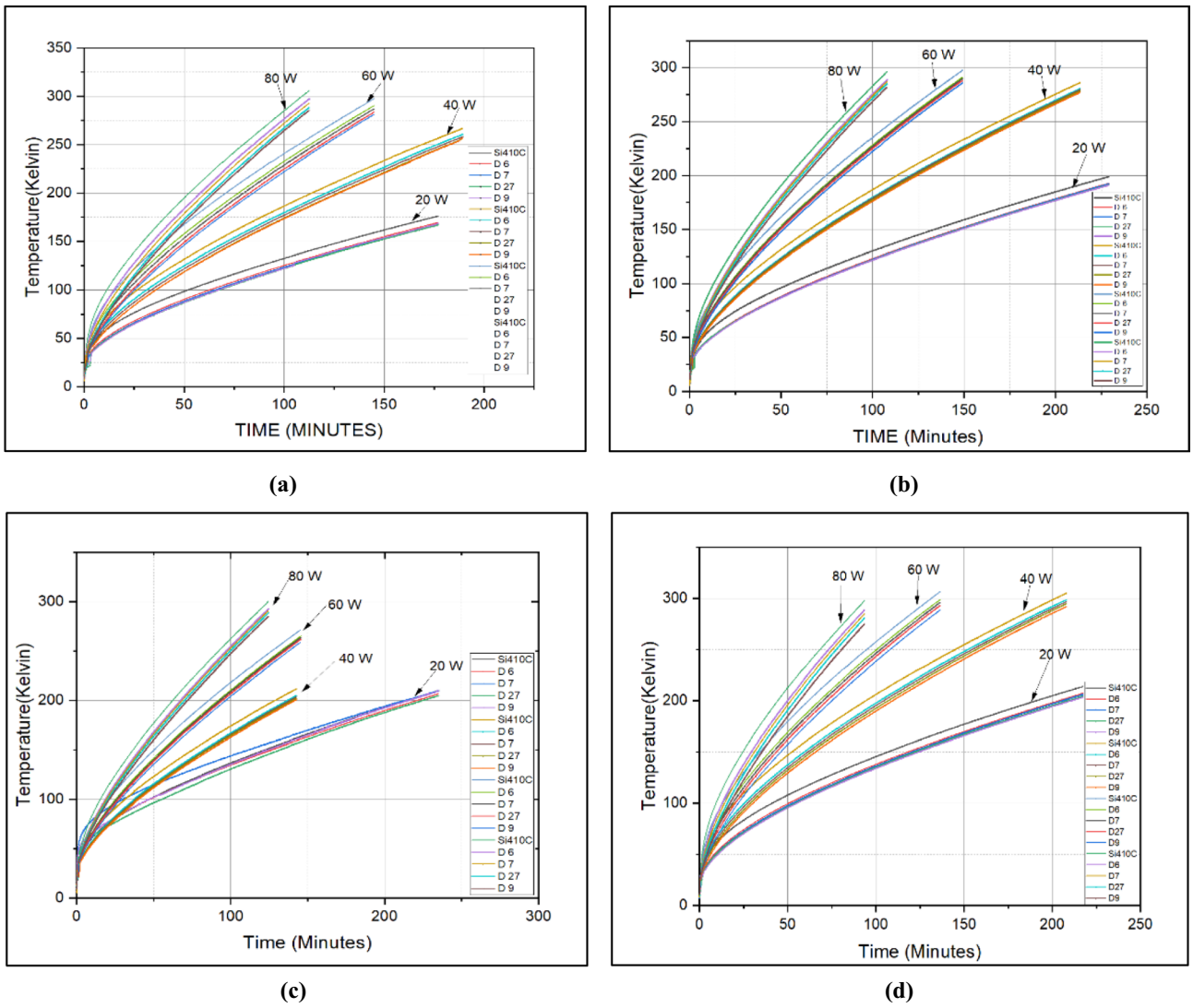

Fig. 11 Experimental warm-up plots for different heat loads—**a** stacked aluminum, **b** stacked copper, **c** stacked Al-Cu, **d** stacked Cu-Al

Table 1 Experimental time taken for cylindrical thermal mass

Heating power	Time required to reach 200 K in minutes					
	Single Al	Single Cu	Stacked Al-Al	Stacked Cu-Cu	Stacked Al-Cu	Stacked Cu-Al
20 W	129.13	177.5	209.97	247.62	219.57	226.79
40 W	71.48	83.64	108.54	128.95	113.99	115.37
60 W	49.36	60.48	65.02	85.95	70.91	74.58
80 W	30.27	36.82	50.49	59.53	52.55	54.57

capacity, C, located below the second-stage cold head as depicted in Fig. 13. This factor was not accounted for in the theoretical analysis. This unaccounted factor contributes to the observed factor F. The thorough consideration of factor F establishes a congruence between theoretical and experimental analyses, affirming their identity.

4.2 Theoretical analysis of different geometric shapes

The examination of experimental and theoretical aspects of cylindrical thermal masses indicated their comparability, particularly regarding the factor denoted as "F." This

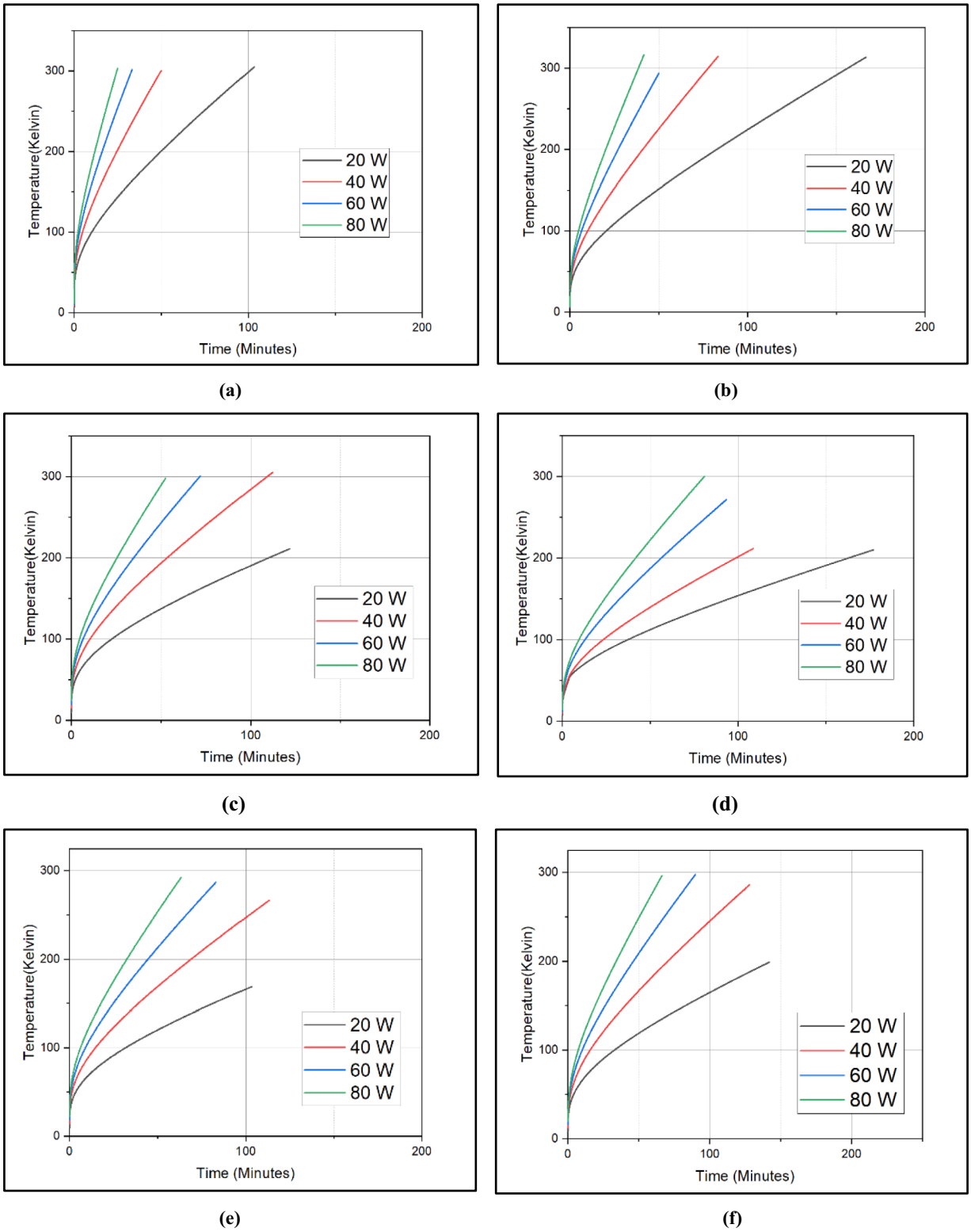

Fig. 12 Theoretical warm-up plots for different heat loads—**a** Aluminum **b** Copper **c** Stacked aluminum **b** Stacked copper **c** Stacked Al-Cu **d** Stacked Cu-Al

Table 2 Theoretical time taken for cylindrical thermal mass

Heating power	Time required to reach 200 K in minutes					
	Single Al	Single Cu	Stacked Al-Al	Stacked Cu-Cu	Stacked Al-Cu	Stacked Cu-Al
20 W	47.36	81.76	120.65	157.72	139.86	140.78
40 W	25.53	40.61	58.65	98.52	68.27	69.08
60 W	17.36	27.01	35.49	55.09	43.66	44.89
80 W	10.67	20.19	28.56	38.58	31.85	33.49

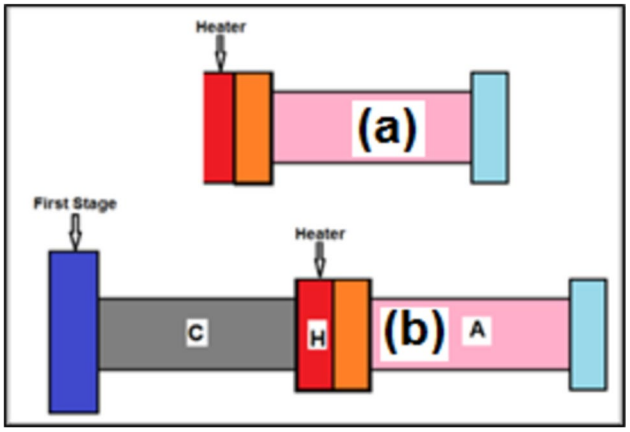

Fig. 13 Schematic representing first and second stage of GM cryo-cooler in theory and in experiment

insight prompted the exploration of experiments involving various geometrical shapes in theoretical studies, presenting a potential time-saving advantage in the fabrication process.

4.2.1 Exploration of different conical and reverse conical shapes

Drawing upon the cylindrical thermal design established, dimensions for diverse arbitrary shapes of thermal masses were created using SolidWorks and CATIA software. The aim was to investigate whether the warm-up behavior of thermal masses is dependent on their shapes. Experimental analyses were conducted by applying an 80 W heat load to observe the resulting warm-up plots, and temperature versus time graphs were subsequently generated.

In consideration of conical structures, one end was fixed at 50 mm, while the other end was varied to dimensions

Table 3 Factor F for different experimental conditions

Heating Power	Al	Cu	Al-Al	Cu-Cu	Al-Cu	Cu-Al
20w	2.74	2.17	1.74	1.57	1.57	1.61
40w	2.81	2.06	1.85	*	1.67	1.67
60w	2.83	2.24	1.83	1.56	1.64	1.66
80w	2.87	*	1.78	1.54	1.65	1.63

Table 4 Deviation for different experimental conditions in terms of percentage

Heating Power	Al	Cu	Al-Al	Cu-Cu	Al-Cu	Cu-Al
20w	±2.58%	±0.61%	±3.33%	±0.85%	±3.83%	±1.98%
40w	±0.09%	±4.48%	±2.77%	*	±2.3%	±1.67%
60w	±0.62%	±3.86%	±1.64%	±0.22%	±0.46%	±1.06%
80w	±2.04%	*	±1.11%	±1.07%	±1.07%	±0.76%

Table 5 Estimation of C values for different experimental conditions

Heating Power	Heat Capacity					
	Cu	Al	Cu-Cu	Al-Al	Cu-Al	Al-Cu
	941	667	1882	1334	1608	1608
	Value of C					
20w	1100.9	1160.9	1072.7	987	980.9	*
40w	997	1207	*	1133.1	1077	1077
60w	1166	1220	1053	1107	1061	1029.5
80w	*	1247	1016	1040.2	1013	1013

of 10 mm, 20 mm, 30 mm, and 40 mm, resulting in the creation of four distinct conical shapes. Additionally, the conical shape was inverted to obtain results for the reverse conical configuration. The warm-up plots for different conical shapes made of aluminum are depicted in Fig. 14a and b, respectively.

The graphical representations above distinctly indicate the nearly identical outcomes for both conical and reverse conical shapes. Table 6 provides the average time, measured in minutes, for the aluminum thermal mass to attain a temperature of 300 K in the conical and reverse conical configurations. Additionally, for comparative purposes, a cylindrical thermal configuration with an end dimension of 50 mm is included. Consequently, the segment with a 50 mm end requires the maximum time for warm-up, while the segment with a 20 mm end necessitates the minimum time for the warm-up process.

The warm-up plots for different conical and reverse conical shapes made of copper are depicted in Fig. 15a and b, respectively. Similar to the aluminum thermal mass, the copper thermal mass exhibits consistent outcomes in the warm-up plots for both conical and reverse conical configurations, as depicted in the graph.

Table 7 further presents the average time, measured in minutes, for the aluminum thermal mass to achieve a temperature of 300 K in the conical and reverse conical setups.

The segment terminating with a 50 mm end exhibits the maximum warm-up time, while the segment concluding with a 20 mm end requires the minimum warm-up time. In comparison with thermal masses composed of aluminum and copper, aluminum demonstrates a reduction of approximately 35% in warm-up time compared to copper across various configurations involving conical and reverse conical shapes. Therefore, the end with a 20 mm termination showcases the minimum warm-up time for both conical and reverse conical shapes. Consequently, this configuration will undergo further analysis to facilitate the comparison of different geometrical shapes.

Table 6 Time taken for different aluminum configuration

Different configuration	Average time taken in minutes for aluminum thermal mass to reach 300 K				
	10 mm	20 mm	30 mm	40 mm	50 mm
Conical	19.72	19.27	21.12	23.36	25.47
Reverse conical	19.54	19.04	20.96	23.27	25.47

4.2.2 Exploration of different geometrical shapes

Utilizing the established cylindrical thermal design as a basis, dimensions were derived for thermal masses of varied arbitrary shapes such as cuboid and sphere (with sphere of 75 mm). A comprehensive comparative analysis was executed to assess thermal masses of different shapes and sizes fabricated from both aluminum and copper. Figure 16 (a) and (b) depicts visual representations of the comparative graphs for aluminum and copper thermal masses, respectively. The graphical representation clearly illustrates that spherical geometrical masses necessitated the longest warm-up time, whereas conical and reverse conical shapes exhibited the shortest heating durations. Intriguingly, both conical and reverse conical shapes yielded comparable results, with the reverse conical shape demonstrating a marginally superior performance. The ascending order of warm-up times is as follows: reverse conical, conical, cuboid, and sphere.

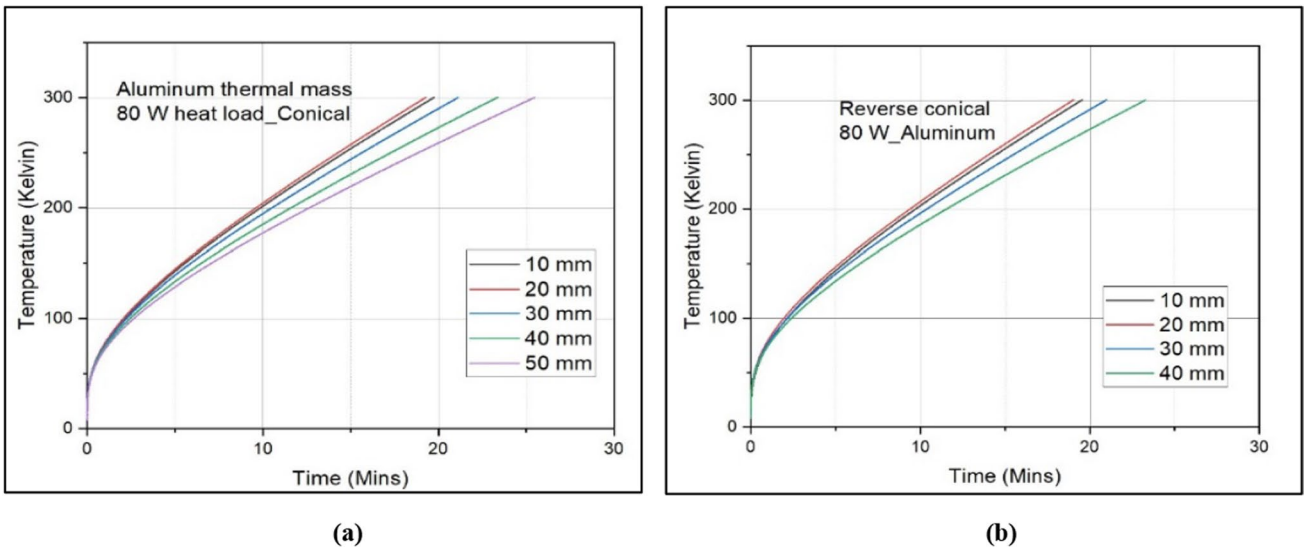

Fig. 14 **a** and **b** conical and reverse conical for aluminum thermal masses

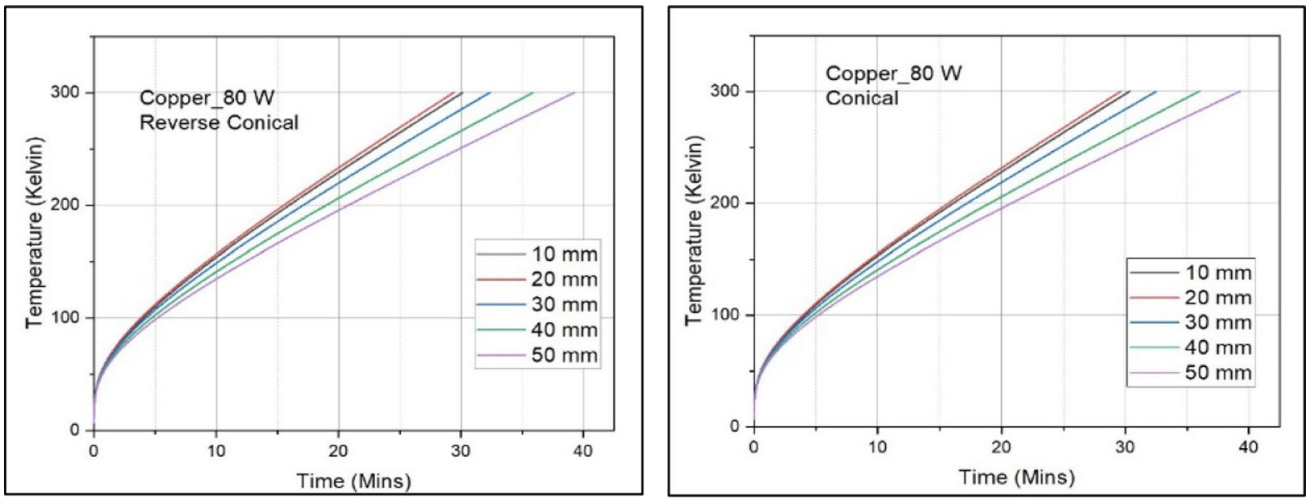

Fig. 15 **a** and **b** conical and reverse conical for copper thermal masses

Table 7 Time taken for different copper configuration

Different configuration	Average time taken in minutes for aluminum thermal mass to reach 300 K				
	10 mm	20 mm	30 mm	40 mm	50 mm
Conical	30.32	29.63	32.5	35.99	39.27
Reverse conical	30.11	29.41	32.37	35.91	39.27

Table 8 presents the average time required to attain a temperature of 300 K during the warm-up process for various geometrical shapes using aluminum and copper materials. Notably, across all diverse geometrical configurations, aluminum thermal masses exhibited an approximately 35% reduction in warm-up time in comparison with copper. Furthermore, the reverse conical shape thermal mass demonstrated an approximately 43% decrease in warm-up time compared to the spherical thermal mass.

This observation highlights the inherent correlation between the warm-up time of a metallic object and its mass, contingent upon a specific geometric configuration. This realization prompted a meticulous comparative analysis of warm-up times across various geometric shapes relative to their masses, encompassing both copper and aluminum materials. To visually articulate these associations, time versus mass graphs were constructed for all thermal masses

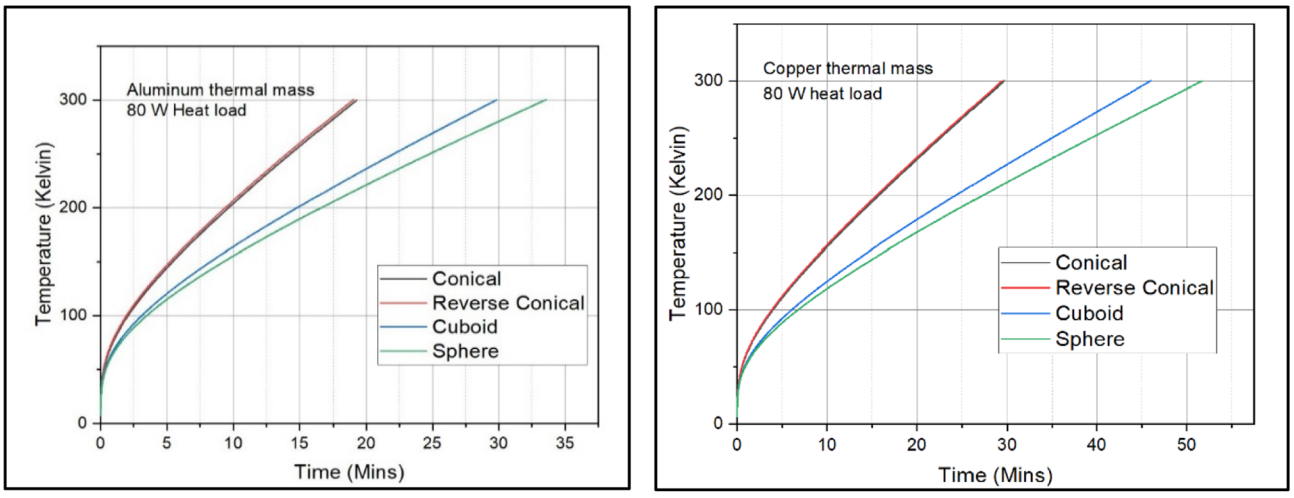

Fig. 16 **a** and **b** Comparison plot of different geometry for aluminum and copper material

Table 8 Time taken for different geometrical shapes

Different material	Average time taken in minutes for different geometrical thermal masses to reach 300 K			
	Reverse conical	Conical	Cuboid	Sphere
Aluminum	19.04	19.27	29.845	33.56
Copper	29.41	29.64	45.98	51.72

within a specified temperature range. Figure 17a illustrates the time versus mass graph for aluminum thermal masses, while Fig. 17b presents the corresponding graph for copper thermal masses. These graphs encompass diverse geometrical shapes, including conical shapes (with 20 mm, 30 mm, and 40 mm ends), cylindrical shapes, cuboidal shapes, and spherical shapes (with spheres of 75 mm and 100 mm).

Both graphs above unveil a fascinating discovery: The warm-up durations of different geometric shapes are intricately linked to the mass of the respective material; be it copper or aluminum. This correlation remains consistent regardless of the specific shape of the object. When we compare materials, such as copper and aluminum, it becomes evident that this correlation is likely influenced by the thermal capacity of the material.

To prove the previous statement, it was assumed that the material has a mass m, and its specific heat be Cp Let Hence the heat input to raise its temperature by dT is given by

$$\mathrm{d}Q = mC_p(T)\mathrm{d}T \tag{5}$$

The total quantity of heat to raise the temperature from T_1 to T_2 is given by

$$Q = \int \mathrm{d}Q = \int_{T1}^{T2} mC_p(T)\mathrm{d}T \tag{6}$$

Since $Q = \text{power} \times \text{time}$, we can calculate the time needed to raise the temp from $T1$ to $T2$ (lower temperature to higher temperature) for a given heater power

$$t_{\text{cal}} = Q/\text{power} \tag{7}$$

For both aluminum and copper thermal masses of 80 W, the warm-up time was evaluated at various temperatures (50 K, 100 K, 150 K, 200 K, and 250 K) for different shapes and sizes. The ANSYS-derived warm-up time, denoted as t_ansys, was used as shown in Fig. 17. Equation 6 was employed to estimate Q, and Eq. 7 was used to calculate t_cal. A MATLAB program was developed to streamline these calculations.

The calculated t_cal values were then compared to the corresponding t_ansys values obtained from the ANSYS analysis. A graphical representation of this comparison is provided in Fig. 18. The results demonstrate a strong correlation between t_cal and t_ansys, suggesting that the warm-up time is primarily influenced by thermal capacity rather than shape or size.

5 Conclusion

- This study presents a systematic investigation of the warm-up process of thermal masses from 4 to 300 K, conducted both experimentally and theoretically.
- The warm-up time of thermal masses is primarily dependent on the wattage of the heat load they are sub-

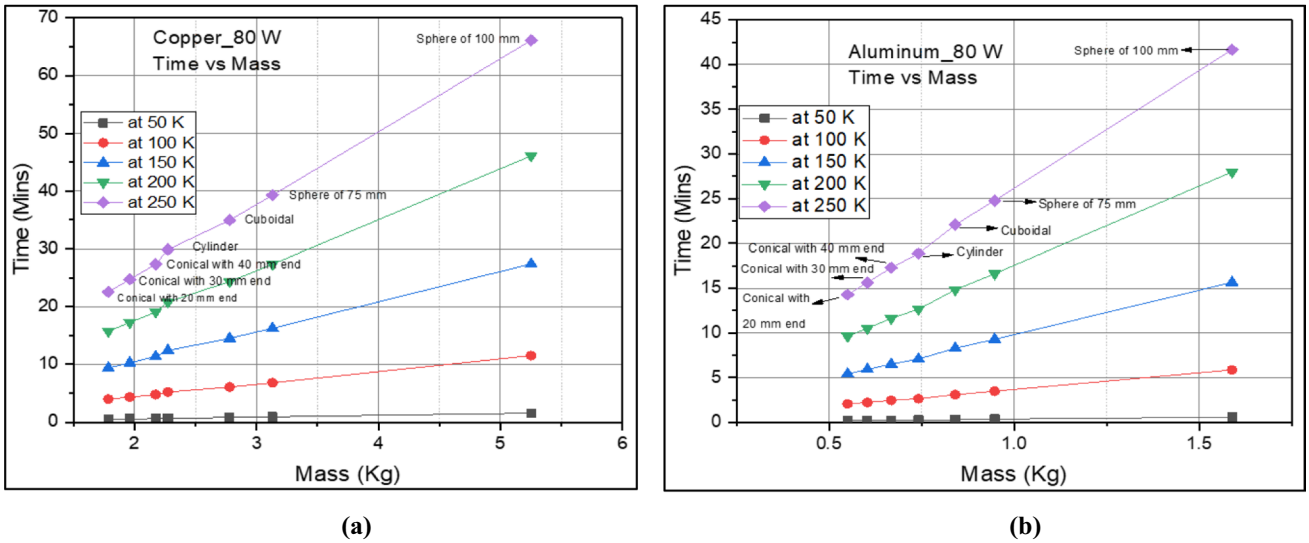

Fig. 17 **a** and **b** Time versus mass of different geometry for aluminum and copper material

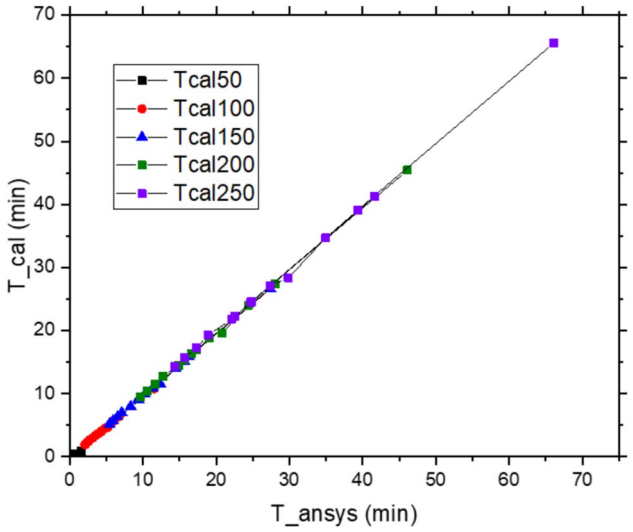

Fig. 18 Plot of *t_cal* versus *t_ansys* for all the thermal masses of copper and aluminum

jected to. Higher heater power enables faster warm-up to a specific temperature compared to a lower heat load. For example, a cylindrical thermal mass with an 80 W heater load warms up four times faster to a specific temperature than one with a 20 W heat load.

- A detailed analysis of the experimental results indicates that the heat capacity of the metal significantly affects its warm-up time. Due to this, the warm-up time of a copper thermal mass is nearly 150% longer than that of an aluminum thermal mass with an identical geometry.
- In our experimental studies, heating occurs not only in the thermal mass attached to the second stage but also in the first stage of a cryocooler. However, this additional heating is not accounted for in the ANSYS simulations. Consequently, the experimental warm-up times are longer than those estimated theoretically. The factor "F," defined as the ratio of $T_{Experimental}/T_{Theoretical}$, has been determined using the thermal capacities of the experimental and theoretical masses. This analysis provides useful insights into thermal masses of various geometries and different metals.
- Our study demonstrates that the warm-up times of thermal masses, regardless of their arbitrary shapes and sizes (characterized by larger specific heat and thermal conductivity), can be estimated based solely on their thermal capacities, independent of their geometries.
- This finding is particularly valuable for estimating the warm-up times of superconducting magnets, assuming they are primarily composed of metals such as copper and aluminum (excluding plastic components). This could have potential applications in future projects, such as the development of portable MRI systems.

Acknowledgements We would like to thank M/s Voxelgrids Innovations Pvt. Ltd. for their assistance in our research work and extend our immense gratitude to QpiAI India Pvt. Ltd. for their constant support for the modification of this paper.

Author contributions Sushanth R Shetty and Ruturaj A. Umaranikar spearheaded the experimental procedures and meticulously collected the data. Shiva Kumar precisely drafted the paper, while Kasthurirengan provided comprehensive oversight throughout the experimental endeavors and also contributed to the finalization of the paper.

Funding Open access funding provided by Manipal Academy of Higher Education, Manipal.

Open Access This article is licensed under a Creative Commons Attribution 4.0 International License, which permits use, sharing, adaptation, distribution and reproduction in any medium or format, as long as you give appropriate credit to the original author(s) and the source, provide a link to the Creative Commons licence, and indicate if changes were made. The images or other third party material in this article are included in the article's Creative Commons licence, unless indicated otherwise in a credit line to the material. If material is not included in the article's Creative Commons licence and your intended use is not permitted by statutory regulation or exceeds the permitted use, you will need to obtain permission directly from the copyright holder. To view a copy of this licence, visit http://creativecommons.org/licenses/by/4.0/.

References

1. Radebaugh R (2009) Cryocoolers: the state of the art and recent developments. J Phys Condens Matter 21:164219
2. Yazdani-Asrami M, Alireza S, Atrey MD (2022) Selecting a cryogenic cooling system for superconducting machines: general considerations for electric machine designers and engineers. Int J Refrig 140:70–81
3. Trevisani L, Kuriyama T, Negrini F, Okamura T, Ohtani Y, Okamura M et al (2022) Performance improvement of a two-stage GM cryocooler by use of Er (Ni0:075Co0:925)2 magnetic regenerator material. Cryogenics 42:653–657
4. Gschneidner KA, Pecharsky AO, Pecharsky VK (2003) Low temperature cryocooler regenerator materials. Cryocoolers 12:457–465
5. Ikeya Y, Li R, Numazawa T (2003) Improvement of 4K GM cooling performance with a new regenerator material. Cryocoolers 12:403–410
6. Bagdinov A, Demikhov E, Kostrov E, Lysenko V, Piskunov N, Rybakov A, Tysyachnykh Y (2017) Performance test of 1.5 T cryogen-free orthopedic MRI magnet. IEEE Trans Appl Supercond 28:1–4
7. Maeda H, Yanagisawa Y (2014) Recent developments in high-temperature superconducting magnet technology (Review). IEEE Trans Appl Supercond 24:1–12
8. Grover VPB, Tognarelli JM, Crossey MM, Cox IJ, Taylor-Robinson SD, McPhail MJ (2015) Magnetic resonance imaging: principles and techniques: lessons for clinicians. J Clin Exp Hepatol 5:246–255
9. Choi YS, Kim DL, Shin DW (2011) Cool-down characteristic of conduction-cooled superconducting magnet by a cryocooler. Phys C Supercond Appl 471:1440–1444
10. Thirumaleshwar M, Subramanyam SV (1989) Gifford-McMahon cycle-a theoretical analysis. Cryogenics 26:178–188

11. Xu M and Longsworth R (2022) Gifford-McMahon Cryocoolers. In: Handbook of Superconductivity, CRC Press. 535–546
12. Radovinsky AL, Michael PC, Zhukovsky A, Forton E, Paradis Y, Nuttens V, Minervini JV (2015) Cold head maintenance with minimal service interruption. In: IOP conference series: materials science and engineering, IOP Publishing. 012181
13. Webber RJ and Delmas J (2015) Cool-down acceleration of GM cryocoolers with thermal oscillations passively damped by helium. In: IOP conference series: materials science and engineering, IOP Publishing. 012137
14. Park J, Ko J, Kim H, Chu S, Kim J, Kim J, In S, Hong Y, Park S, Yeom H (2022) Development of a large capacity cryopump equipped with a two-stage GM cryocooler. Appl Therm Eng 217:119217
15. Ackermann RA, Herd KG and Chen WE (1999) In: Advanced Cryocooler cooling for MRI systems, Boston, Cryocoolers. 857–867
16. Wang C, Olesh A, Cosco J (2017) Performance improvement of a large capacity GM cryocooler. IOP Conf Ser Mater Sci Eng 278:012166
17. Wang C, Hanrahan T and Cosco J (2018) A large single-stage GM cryocooler for operating temperatures of 13–30 K. In: Proceedings of 20th International Cryocooler Conference, Burlington Vermont
18. Li J, Zheng H, Cheng Z, Li L, Wang Q, Song Y (2024) Thermal analysis of a head-only 1.5 T magnetic resonance imaging superconducting magnet. IEEE Trans Appl Supercond 34:5
19. Wang Y, Wang S, Liang P, Brusic V, Zeng J, Liu B, Wang C (2023) Design, construction and performance testing of a 15 T cryogen-free low-temperature superconductor whole-body. MRI Magnet Supercond Sci Technol 36:045022
20. Chao W, Li R, Zhao Q, Li A, Zhou Z, He H, Wang B, Gan Z (2024) A high capacity GM cryocooler working at liquid helium temperatures for horizontal operation. Appl Therm Eng 244:122765
21. Qu H, Wu H, Qu H, Wu H (2024) A 1.5T liquid-helium-free whole-body MRI superconducting magnet: thermal analysis and cool-down time estimation. IEEE International conference on applied superconductivity and electromagnetic devices (ASEMD)
22. Kumar K, Kumar R, Bharj RS (2023) Entropy generation studies of turbulent fluid flow through novel hybrid corrugated channels with variable thermophysical properties. Int J Modern Phys 37:26
23. Kumar K, Kumar R, Bharj RS (2022) Effect of arc corrugation initiation on the thermo-hydraulic performance and entropy generation of the corrugated tube. Int Commun Heat Mass Transfer 138:106335

Publisher's Note Springer Nature remains neutral with regard to jurisdictional claims in published maps and institutional affiliations.